Comparison of Asymptotic Backscattering Models (SSA, WCA, and LCA) From One-Dimensional Gaussian Ocean-Like Surfaces

Christophe Bourlier, *Member, IEEE*, Nicolas Déchamps, and Gérard Berginc

***Abstract*—In this paper, recent asymptotic backscattering models are compared for one-dimensional multiscale dielectric sea surfaces with Gaussian statistics and by considering the Elfouhaily *et al.* height spectrum. We focus on the calculations of the normalized radar cross sections (NRCS) obtained from the weighted and local curvature approximations (WCA and LCA), recently published by Elfouhaily, and of the first- and second-order small slope approximation (SSA(1) plus SSA(2) denoted as SSA), developed by Voronovich. Voronovich *et al.* (2002 Waves Random Media 11 247–269) presented simulations of the SSA by making an assumption over the SSA(2) contribution (the model is referred to as SSAM). The NRCS computation is then similar to SSA(1), where the sea spectrum is substituted by a modified spectrum defined as the product of the sea spectrum by the second-order polarization term. The second-order statistical moment of WCA is calculated rigorously for any two-dimensional height correlation of the surface with Gaussian statistics. The NRCS of the WCA, WCAQ (obtained from a quadratic approximation of WCA), LCA, SSA, and SSAM backscattering models are compared for moderate wind speeds, for microwave frequencies and for backscattering angles ranging from 0 (nadir) to 70°.**

***Index Terms*—Radar scattering, ocean remote sensing, scattering from rough surface.**

I. Introduction

THE most widely used method to calculate the microwave backscattering from multiscale sea surfaces is the two-scale model (TSM) derived for acoustic waves by Kur'yanov [1] and for electromagnetic waves by Wright [2]. It introduces a scale-dividing parameter k_d separating the small- and large-scale components of the roughness which can be arbitrarily chosen within wide limits. The advantage of this method is that it is easy to apply. One disadvantage is that the predictions are dependent on the partitioning of the surface within the choice of k_d. A second one is the difficulty in establishing the accuracy of the theory.

The first- and second-order small slope approximation (SSA(1) and SSA(2) denoted as SSA) developed by Voronovich [3]–[5] can be applied for rough multiscale surfaces such as the sea surface, since its domain of validity is independent of the electromagnetic wavelength. Indeed, Voronovich showed in [6] that the higher-oder SSA captures the two scale model. The SSA scattering model can be applied when the slopes of the incident and scattered fields sufficiently exceed the rms (root mean square) slopes of the surface. The applicability of the SSA model to scattering from ocean-like surfaces at microwave frequencies has not been fully established. Nevertheless, when the difference between the first- and second-order results is relatively small, one may hope that the solution of the scattering problem is accurate.

The weighted curvature approximation (WCA), recently published by Elfouhaily *et al.* [7], is a new version of the extended Kirchhoff approximation published by Elfouhaily *et al.* [8], which has been compared in [9] with the first-order SSA and also with direct numerical simulations using the MOMI method. WCA can be considered as a generalization of the local weight approximation by Dashen and Wurmser [10]. This model satisfies the necessary conditions of convergence toward the small perturbation method and the high-frequency Kirchhoff approximation while remaining compact, reciprocal an tilt invariant. Therefore, it should be also adequate for multiscale rough surfaces. The local curvature approximation (LCA), recently published by Elfouhaily *et al.* [7], [11], [12], can be seen as a generalization of the tilt-invariant approximation [13], [14], valid only for a metallic surface, to the dielectric case. Like WCA, it is reciprocal, tilt invariant and converges toward the small perturbation method and the high-frequency Kirchhoff approximation.

For radar microwave applications (frequency range from 1 to 20 GHz corresponding to electromagnetic wave number range from 21 to 419 rad/m), the Rayleigh parameter of the sea surface can be much greater than unity. In addition, the sea has a wide-band spectrum involving that the calculation of the height correlation, obtained by computing the IFFT of the spectrum, requires a great number of samples which increases the computing time. Indeed, the height correlation has to take into account information on both the gravity waves (related to the low frequencies) and the capillary waves (related to the high frequencies) to reproduce the two-scale model. These points make its difficult the numerical computation of the multidimensional integrals of the normalized radar cross section (NRCS). To have a short computing time and to study the scattering models with accuracy, the sea surface is then assumed to be one-dimensional (1-D).

Manuscript received May 11, 2004; revised September 18, 2004.

C. Bourlier is with the Institut de Recherche en Electrotechnique et Electronique de Nantes Atlantique (IREENA), Ecole polytechnique de l'université de Nantes, 44306 Nantes, France (e-mail: christophe.bourlier@polytech.univ-nantes.fr).

N. Déchamps was with the Institut de Recherche en Electrotechnique et Electronique de Nantes Atlantique (IREENA), Ecole polytechnique de l'université de Nantes, 44306 Nantes, France. He is now with the Department of Chemical Engineering and Applied Chemistry, University of Toronto, Toronto, ON M5S 3E5, Canada.

G. Berginc is with Thalès Optronique, 78283 Guyancourt, France.

Digital Object Identifier 10.1109/TAP.2005.846800

The purpose of this paper is to compare SSA with WCA and LCA at microwave frequencies and for moderate wind speeds from 1-D Gaussian rough multiscale sea surfaces that obeys the Elfouhaily *et al.* [15] height spectrum. In addition, the modified SSA model used by Voronovich *et al.* [3] and referred to as SSAM will be presented. The ensemble average of the WCA scattered field is calculated by assuming Gaussian statistics. A quadratic approximation, referred to as WCAQ and suggested by Dr. Elfouhaily (personal discussion) is applied to simplify the scattering cross section of the WCA model.

This paper is organized as follows. In Section II, the SSA, SSAM, LCA, WCA, and WCAQ scattering models are presented. In Section III, by assuming a height spectrum given by [15], the backscattering models are compared for a wind speed $u_{10} = 5$ m/s (defined at ten meters above the sea), for a radar frequency $f = 14$ GHz (*Ku* band) and for backscattering angles ranging from 0° (nadir) to 70°. The last section briefly discusses results for other frequencies and ocean states, and provides concluding remarks.

II. SSA, WCA, and LCA Scattering Models

A. SSA Approach

The SSA scattering model has been analytically tested in many papers that considered Gaussian statistics to derive expressions for ensemble averages. For a 2-D ocean-like surface, the comparison [16], [17] of the SSA(1) backscattering NRCS with experimental data showed good agreement. In [18], only the SSA cross term of the backscattering NRCS is added (the partial fourth order term is omitted). In [3], an assumption is used to include the SSA(2). The computation of the SSA backscattering NRCS becomes then similar to the computation of the SSA(1) NRCS, where the sea spectrum is substituted by a modified spectrum which depends on the sea spectrum and the second-order polarization terms. This model will be presented and referred to as SSAM. In [19], SSA(1) is compared with a rigorous numerical code based on the method of moments for Gaussian and power-law spectra. For a 1-D Dirichlet surface with a Gaussian elevation spectrum (single-scale surface), the comparison of the SSA bistatic NRCS with the method of Moments showed good agreement [20], and similar simulations are reported in [21], [22] for ocean-like dielectric surfaces. Recently, Berginc [23] and Gilbert *et al.* [24] implemented numerically the vector case of SSA from 2-D dielectric surfaces with a Gaussian height spectrum. This list of references is not exhaustive.

The SSA presents an explicit expression of the scattering amplitude (SA) $S(\mathbf{k},\mathbf{k}_0)$ on the basis of plane waves in terms of parameters of the incident and the scattered waves and surface roughness elevation $h(\mathbf{r})$ [4], [5]

$$S(\mathbf{k},\mathbf{k}_0) = \frac{2(q_k q_0)^{\frac{1}{2}}}{Q}\int \exp[-j\mathbf{q}_H\cdot\mathbf{r} + jQh(\mathbf{r})] \times\left[B(\mathbf{k},\mathbf{k}_0) - \frac{j}{4}\int \hat{M}(\mathbf{k},\mathbf{k}_0;\mathbf{u})\hat{h}(\mathbf{u}) \times \exp(j\mathbf{u}\cdot\mathbf{r})\,d\mathbf{u}\right]\frac{d\mathbf{r}}{(2\pi)^2} \quad (1)$$

where

$$Q = q_k + q_0 \quad \text{and} \quad \mathbf{q}_H = \mathbf{k} - \mathbf{k}_0. \quad (2)$$

In (1), $\mathbf{r} = (x, y)$ are the horizontal coordinates and $\{\mathbf{k}_0, \mathbf{k}\}$ are the horizontal projections of the incident and scattered wave vectors, correspondingly, and $\hat{h}(\mathbf{u})$ is the Fourier transform of $h(\mathbf{r})$. Values $-q_0$ and q_k are appropriate vertical projections of the wavevectors defined as

$$q_0 = \left(K^2 - \mathbf{k}_0^2\right)^{\frac{1}{2}} \text{ and } q_k = (K^2 - \mathbf{k}^2)^{\frac{1}{2}} \quad (3)$$

where $\Im m(q_0, q_k) \geq 0$, and

$$\hat{M}(\mathbf{k},\mathbf{k}_0;\mathbf{u}) = \hat{B}_2(\mathbf{k},\mathbf{k}_0;\mathbf{k}-\mathbf{u}) + \hat{B}_2(\mathbf{k},\mathbf{k}_0;\mathbf{k}_0+\mathbf{u}) + 2QB(\mathbf{k},\mathbf{k}_0). \quad (4)$$

SA $S(\mathbf{k},\mathbf{k}_0)$ represents a 2×2 matrix describing mutual transformations of the electromagnetic waves at different polarizations. Namely, $S_{\alpha\alpha_0}(\mathbf{k},\mathbf{k}_0)$ is the amplitude of the scattering from an incident plane wave with horizontal wavevector $\mathbf{k}_0$ and polarization $\alpha_0 = \{1, 2\}$ into a scattered plane wave with horizontal wavevector $\mathbf{k}$ and polarization $\alpha = \{1, 2\}$. In our case, the polarization index $\alpha = 1$ corresponds to a polarization conventionally defined as vertical, and $\alpha = 2$ refers to a horizontal polarization. Values $B_{\alpha\alpha_0}$, $\hat{B}_{2,\alpha\alpha_0}$ are expressed in Appendix B and $\hat{M}_{\alpha\alpha_0}$ are 2×2 matrices.

The expression of the scattering cross section is directly related to the second-order statistical moment of the SA. For a Gaussian process [4], [5], the dimensionless scattering cross section $\sigma^{\mathrm{SSA}}_{\alpha\alpha_0}(\mathbf{k},\mathbf{k}_0)$ for the scattering of the wave of polarization α_0 into the wave of polarization α is

$$\sigma^{\mathrm{SSA}}_{\alpha\alpha_0}(\mathbf{k},\mathbf{k}_0) = \left(\frac{2q_k q_0}{Q}\right)^2 \int R^{\mathrm{SSA}}_{\alpha\alpha_0}(\mathbf{k},\mathbf{k}_0;\mathbf{r}) e^{-j\mathbf{q}_H\cdot\mathbf{r}}\frac{d\mathbf{r}}{(2\pi)^2} \quad (5)$$

where

$$R^{\mathrm{SSA}}_{\alpha\alpha_0}(\mathbf{r}) = R^{\mathrm{SSA11}}_{\alpha\alpha_0}(\mathbf{r}) + R^{\mathrm{SSA12}}_{\alpha\alpha_0}(\mathbf{r}) + R^{\mathrm{SSA22}}_{\alpha\alpha_0}(\mathbf{r}) \quad (6)$$

in which

$$R^{\mathrm{SSA11}}(\mathbf{r}) = [\chi(\mathbf{r}) - \chi(\infty)]\,|B|^2 \quad (7)$$

$$R^{\mathrm{SSA12}}(\mathbf{r}) = \chi(\mathbf{r})\,[F_1(\mathbf{r})B^* + F_1^*(-\mathbf{r})B + F_1(\mathbf{r})F_1^*(-\mathbf{r})] - \chi(\infty)\{|F(\mathbf{0})|^2 - 2\Re e[F(\mathbf{0})B^*]\} \quad (8)$$

$$R^{\mathrm{SSA22}}(\mathbf{r}) = \chi(\mathbf{r})G(\mathbf{r}) \quad (9)$$

$$\chi(\mathbf{r}) = e^{-Q^2\left[\sigma_h^2 - W(\mathbf{r})\right]}, \quad \chi(\infty) = e^{-Q^2\sigma_h^2} \quad (10)$$

$$F_1(\mathbf{r}) = F(-\mathbf{r}) - F(\mathbf{0}). \quad (11)$$

The symbol $*$ stands for the complex conjugate and the symbol $\Re e$ denotes the real part. In (7)–(9) and (11), the subscript $\alpha\alpha_0$ and the dependence over $(\mathbf{k},\mathbf{k}_0)$ of $R^{\mathrm{SSA11}}, R^{\mathrm{SSA12}}, R^{\mathrm{SSA22}}, B, F, F_1$, and G are omitted. $\chi(\mathbf{r})$ is the characteristic function; and the height correlation, $W(\mathbf{r})$, is defined from its height spectrum, $\hat{W}(\mathbf{u})$, as

$$W(\mathbf{r}) = \int \hat{W}(\mathbf{u})\exp(j\mathbf{u}\cdot\mathbf{r})\,d\mathbf{u}. \quad (12)$$

The height variance is defined as $\sigma_h^2 = W(\mathbf{0})$. In (11) and (9), $F(\mathbf{r}) \equiv F_{\alpha\alpha_0}(\mathbf{k},\mathbf{k}_0;\mathbf{r})$ and $G(\mathbf{r}) \equiv G_{\alpha\alpha_0}(\mathbf{k},\mathbf{k}_0;\mathbf{r})$ are expressed as

$$F_{\alpha\alpha_0}(\mathbf{r}) = \frac{Q}{4}\int \hat{W}(\mathbf{u})\hat{M}_{\alpha\alpha_0}(\mathbf{k},\mathbf{k}_0;\mathbf{u})\exp(j\mathbf{u}\cdot\mathbf{r})d\mathbf{u} \quad (13)$$

$$G_{\alpha\alpha_0}(\mathbf{r}) = \frac{1}{16}\int \hat{W}(\mathbf{u})|\hat{M}_{\alpha\alpha_0}(\mathbf{k},\mathbf{k}_0;\mathbf{u})|^2\exp(j\mathbf{u}\cdot\mathbf{r})\,d\mathbf{u}. \quad (14)$$

$R_{\alpha\alpha_0}^{\mathrm{SSA11}}(\mathbf{r}), R_{\alpha\alpha_0}^{\mathrm{SSA12}}(\mathbf{r})$, and $R_{\alpha\alpha_0}^{\mathrm{SSA22}}(\mathbf{r})$ are related to the second (superscript 11), third (superscript 12), and partial fourth (superscript 22) order terms of the scattering cross section, respectively. Thus, the SSA method requires to compute three Inverse fast Fourier transform (IFFT) to obtain $\hat{W}(\mathbf{u}), F_{\alpha\alpha_0}(\mathbf{k},\mathbf{k}_0;\mathbf{r}), G_{\alpha\alpha_0}(\mathbf{k},\mathbf{k}_0;\mathbf{r})$ and a numerical integration over $\mathbf{r}$. For a multiscale sea surface, for which the height spectrum is very wide and the Rayleigh parameter (proportional to the product of the electromagnetic wave number by the surface rms height) is much greater than unity at microwave frequencies, the computation of the IFFTs are much more difficult since the sampling of the spectrum must be sufficiently small to take into account both the gravity and the capillary waves. This is why, for the simulations, the surface is assumed to be 1-D, for which the V and H polarization contributions will be displayed.

B. SSAM Approach

To facilitate the calculations in the cases of the SSA12 and SSA22, Voronovich *et al.* [3] assumed in (1) that

$$B - \frac{j}{4}\int \hat{M}(\mathbf{u})\hat{h}(\mathbf{u})\exp(j\mathbf{u}\cdot\mathbf{r})\,d\mathbf{u} \approx B\times\exp\left[-\frac{j}{4B}\int \hat{M}(\mathbf{u})\hat{h}(\mathbf{u})\exp(j\mathbf{u}\cdot\mathbf{r})\,d\mathbf{u}\right]. \quad (15)$$

Thus, they showed

$$\sigma_{\alpha\alpha_0}^{\mathrm{SSAM}}(\mathbf{k},\mathbf{k}_0) = \left(\frac{2q_kq_0}{Q}\right)^2 \times\int R_{\alpha\alpha_0}^{\mathrm{SSAM}}(\mathbf{k},\mathbf{k}_0;\mathbf{r})e^{-j\mathbf{q}_H\cdot\mathbf{r}}\frac{d\mathbf{r}}{(2\pi)^2} \quad (16)$$

where

$$R_{\alpha\alpha_0}^{\mathrm{SSAM}}(\mathbf{r}) = |B_{\alpha\alpha_0}|^2 e^{-Q^2\Re e[W_{\alpha\alpha_0}(\mathbf{0})-W_{\alpha\alpha_0}(\mathbf{r})]}. \quad (17)$$

$W_{\alpha\alpha_0}(\mathbf{r}) \equiv W_{\alpha\alpha_0}(\mathbf{k},\mathbf{k}_0;\mathbf{r})$ is related to the modified roughness spectrum $\hat{W}_{\alpha\alpha_0}(\mathbf{k},\mathbf{k}_0;\mathbf{u})$ as

$$W_{\alpha\alpha_0}(\mathbf{k},\mathbf{k}_0;\mathbf{r}) = \int \hat{W}_{\alpha\alpha_0}(\mathbf{k},\mathbf{k}_0;\mathbf{u})\exp(j\mathbf{u}\cdot\mathbf{r})\,d\mathbf{u} \quad (18)$$

where

$$\hat{W}_{\alpha\alpha_0}(\mathbf{k},\mathbf{k}_0;\mathbf{u}) = \hat{W}(\mathbf{u})\left|1-\frac{\hat{M}_{\alpha\alpha_0}(\mathbf{k},\mathbf{k}_0;\mathbf{u})}{4QB_{\alpha\alpha_0}(\mathbf{k},\mathbf{k}_0)}\right|^2. \quad (19)$$

Equation (16) is similar to that giving the contribution of the SSA11 where the height correlation $W(\mathbf{r})$ was substituted by $W_{\alpha\alpha_0}(\mathbf{r})$.

C. WCA Model

1) Weighted Curvature Approximation: The WCA is based on the curvature kernel derived in the local curvature approximation developed for the electromagnetic case by Elfouhaily *et al.* [7]. It is formulated as

$$S(\mathbf{k},\mathbf{k}_0) = \frac{1}{Q}\int \exp[-j\mathbf{q}_H\cdot\mathbf{r}+jQh(\mathbf{r})] \times[B_E(\mathbf{w}_H,\mathbf{q}_H) - T(\mathbf{w}_H,-Q\boldsymbol{\nabla}h)]\frac{d\mathbf{r}}{(2\pi)^2} \quad (20)$$

where

$$T(\mathbf{w}_H,\mathbf{u}) = B_E(\mathbf{w}_H,\mathbf{u}) - K_E(\mathbf{w}_H,\mathbf{u}) \quad (21)$$

and $B_E(\mathbf{w}_H,\mathbf{q}_H) \equiv B_E(\mathbf{k},\mathbf{k}_0), K_E(\mathbf{w}_H,\mathbf{q}_H) \equiv K_E(\mathbf{k},\mathbf{k}_0), T(\mathbf{w}_H,\mathbf{q}_H) \equiv T(\mathbf{k},\mathbf{k}_0)$, in which $\mathbf{q}_H = \mathbf{k}-\mathbf{k}_0$ and $\mathbf{w}_H = \mathbf{k}+\mathbf{k}_0$. The coefficient K_E is the Kirchhoff polarization matrix given in Appendix B and B_E is related to the polarization matrix B of SSA(1) as $B_E(\mathbf{k},\mathbf{k}_0) = 2q_kq_0B(\mathbf{k},\mathbf{k}_0)$. The definition of the curvature kernel T ensures the high-frequency limit obtained from the Kirchhoff approximation. In addition, since $T(\mathbf{w}_H,\mathbf{0}) = 0$ and $\boldsymbol{\nabla}T(\mathbf{w}_H,\mathbf{0}) = 0, T$ is quadratic in its lower order and therefore the small perturbation method is reached.

2) Calculation of the Ensemble Average: In this paper, we propose to calculate rigorously the ensemble average $\Delta S(\mathbf{k},\mathbf{k}_0) = \langle S(\mathbf{k},\mathbf{k}_0)S^*(\mathbf{k},\mathbf{k}_0)\rangle$ (in the functional $S,\mathbf{r}$ is substituted by $\mathbf{r}_1$ whereas in $S^*,\mathbf{r}$ is substituted by $\mathbf{r}_2$) to obtain $\sigma_{\alpha\alpha_0}^{\mathrm{WCA}}$.

Equation (20) is split up into two terms as $S(\mathbf{k},\mathbf{k}_0) = S_1(\mathbf{k},\mathbf{k}_0) + S_2(\mathbf{k},\mathbf{k}_0)$, where $S_1(\mathbf{k},\mathbf{k}_0)$ includes only $B_E(\mathbf{w}_H,\mathbf{q}_H)$, whereas $S_2(\mathbf{k},\mathbf{k}_0)$ includes only $T(\mathbf{w}_H,-Q\boldsymbol{\nabla}h)$. Thus, we get

$$\Delta S = \langle S_1S_1^*\rangle + \langle S_2S_2^*\rangle - 2\Re e[\langle S_1S_2^*\rangle] - \{|\langle S_1\rangle|^2 + |\langle S_2\rangle|^2 - 2\Re e[\langle S_1\rangle\langle S_2^*\rangle]\}. \quad (22)$$

For a stationary surface or spatially homogeneous surface, the ensemble average $\langle\cdots\rangle$ depends only on the difference $\mathbf{r} = \mathbf{r}_2-\mathbf{r}_1$. Therefore, using the variables transformations $\mathbf{r} = \mathbf{r}_2-\mathbf{r}_1, \mathbf{r}_p = \mathbf{r}_2+\mathbf{r}_1$, and integrating over $\mathbf{r}_p$, we have

$$\langle S_1S_1^*\rangle = \frac{|B_E|^2}{Q^2}\int \mathcal{L}(1)e^{j\mathbf{q}_H\cdot\mathbf{r}}\frac{d\mathbf{r}}{(2\pi)^4} \quad (23)$$

$$\langle S_1S_2^*\rangle = \frac{|B_E|^2}{Q^2}\int \mathcal{L}[T^*(\mathbf{w}_H,-Q\boldsymbol{\nabla}h_2)]e^{j\mathbf{q}_H\cdot\mathbf{r}}\frac{d\mathbf{r}}{(2\pi)^4} \quad (24)$$

$$\langle S_2S_2^*\rangle = \frac{|B_E|^2}{Q^2}\int \mathcal{L}[T^*(\mathbf{w}_H,-Q\boldsymbol{\nabla}h_2) \times T(\mathbf{w}_H,-Q\boldsymbol{\nabla}h_1)]e^{j\mathbf{q}_H\cdot\mathbf{r}}\frac{d\mathbf{r}}{(2\pi)^4} \quad (25)$$

where $\mathcal{L}(\ldots)$ is the statistical operator defined as

$$\mathcal{L}(\cdots) = \langle (\cdots) \exp[jQ(h_2 - h_1)] \rangle \quad \text{where } \mathcal{L}(1) = \chi(\mathbf{r}) \tag{26}$$

for a Gaussian process. The statistical moments $|\langle S_1 \rangle|^2, |\langle S_2 \rangle|^2$, and $\langle S_1 \rangle \langle S_2^* \rangle$ giving the coherent contributions are obtained from (23)–(25) by omitting the statistic correlation (similar to $\mathbf{r} \to \infty$). The calculation of the expected values are presented in the Appendix A for Gaussian statistics and for any 2-D anisotropic correlation. The resulting scattering cross section is

$$\sigma_{\alpha\alpha_0}^{\mathrm{WCA}}(\mathbf{k}, \mathbf{k}_0) = \frac{1}{Q^2} \int R_{\alpha\alpha_0}^{\mathrm{WCA}}(\mathbf{k}, \mathbf{k}_0; \mathbf{r}) e^{-j\mathbf{q}_H \cdot \mathbf{r}} \frac{d\mathbf{r}}{(2\pi)^2} \tag{27}$$

where

$$R_{\alpha\alpha_0}^{\mathrm{WCA}}(\mathbf{r}) = R_{\alpha\alpha_0}^{\mathrm{WCA11}}(\mathbf{r}) + R_{\alpha\alpha_0}^{\mathrm{WCA12}}(\mathbf{r}) + R_{\alpha\alpha_0}^{\mathrm{WCA22}}(\mathbf{r}) \tag{28}$$

in which

$$R^{\mathrm{WCA11}}(\mathbf{r}) = [\chi(\mathbf{r}) - \chi(\infty)]|B_E|^2 \tag{29}$$

$$R^{\mathrm{WCA12}}(\mathbf{r}) = -2\Re e\{B_E[L_{12}(\mathbf{r}) - L_{12}(\infty)]\} \tag{30}$$

$$R^{\mathrm{WCA22}}(\mathbf{r}) = L_{22}(\mathbf{r}) - L_{22}(\infty). \tag{31}$$

The functions $L_{12}(\mathbf{r}) \equiv L_{12,\alpha\alpha_0}(Q, \mathbf{w}_H; \mathbf{r})$ and $L_{22}(\mathbf{r}) \equiv L_{22,\alpha\alpha_0}(Q, \mathbf{w}_H; \mathbf{r})$ are expressed from (A19) and (A14), and $\{L_{12,22}(\infty) \equiv L_{12,22}^{\infty}\}$ are expressed from (A18) and (A23). When the ensemble average is calculated rigorously, two additional integrations over $\{\nabla h_1, \nabla h_2\}$ are required for $L_{22,\alpha\alpha_0}(Q, \mathbf{w}_H; \mathbf{r})$, whereas for $L_{12,\alpha\alpha_0}(Q, \mathbf{w}_H; \mathbf{r})$ one additional integration over ∇h_1 is required. For a 1-D surface, the slopes $\{\nabla h_i\}$ become scalar, which reduces the number of integrations. Comparing (29) with (7) where $B_E = 2q_k q_0 B$, we have $\sigma_{\alpha\alpha_0}^{\mathrm{WCA11}} = \sigma_{\alpha\alpha_0}^{\mathrm{SSA11}}$. $\sigma_{\alpha\alpha_0}^{\mathrm{SSA11,WCA11}}$ are related to $R_{\alpha\alpha_0}^{\mathrm{SSA11,WCA11}}$.

3) Calculation of the Ensemble Average Based on the Quadratic Assumption: To reduce the number of the numerical integrations of $\sigma_{\alpha\alpha_0}^{\mathrm{WCA}}$, we can use a quadratic assumption (suggested by Dr. Elfouhaily) of the curvature kernel $T(\mathbf{w}_H, \mathbf{u})$. Indeed, since T is quadratic with respect to $\mathbf{u}$ in its lower order, a Taylor series expansion of second order around zero leads to $T(\mathbf{w}_H, \mathbf{u}) \approx \mathbf{u} A \mathbf{u}$. It is easy to show that the resulting ensemble average (the superscript Q is added) of (20) is

$$\sigma_{\alpha\alpha_0}^{\mathrm{WCA}Q}(\mathbf{k}, \mathbf{k}_0) = \frac{1}{Q^2} \int R_{\alpha\alpha_0}^{\mathrm{WCA}Q}(\mathbf{k}, \mathbf{k}_0; \mathbf{r}) e^{-j\mathbf{q}_H \cdot \mathbf{r}} \frac{d\mathbf{r}}{(2\pi)^2} \tag{32}$$

where

$$R_{\alpha\alpha_0}^{\mathrm{WCA}Q}(\mathbf{r}) = \chi(\mathbf{r})|B_E - T(\mathbf{w}_H, \mathbf{v})|^2 - \chi(\infty)|B_E - T(\mathbf{w}_H, \mathbf{v}[\infty])|^2 \tag{33}$$

in which

$$\mathbf{v}(\mathbf{r}) = Q\{[Q\nabla W(\mathbf{r})]^2 - \nabla\nabla W(\mathbf{0})\}^{\frac{1}{2}}$$

and

$$\mathbf{v}(\infty) = Q[-\nabla\nabla W(\mathbf{0})]^{\frac{1}{2}}. \tag{34}$$

We can notice that the computation of $\sigma_{\alpha\alpha_0}^{\mathrm{WCAQ}}$ requires a single integration over $\mathbf{r}$ instead of three over $\{\mathbf{r}, \nabla h_1, \nabla h_2\}$ for $\sigma_{\alpha\alpha_0}^{\mathrm{WCA}}$.

4) Application to a 1-D Surface: For a 1-D surface, the surface slope is defined along one direction ($\mathbf{r} \equiv x, \mathbf{w}_H \equiv w_H, \mathbf{q}_H \equiv q_H$ and the vectorial notation disappears) which means that $\nabla h_i \equiv \gamma_i$. Thus, we get from Appendix

$$L_{22} = \int\int T^*(w_H, -Q\gamma_2) T(w_H, -Q\gamma_1) \times \exp\left(-\frac{Q^2}{4a} + jQ\alpha\right) p_{2s}(\gamma_1, \gamma_2) d\gamma_1 d\gamma_2 \tag{35}$$

where

$$\begin{cases} \alpha = -W_1(\gamma_1 + \gamma_2)\left(\sigma_s^2 - W_2\right)^{-1} \\ (4a)^{-1} = \sigma_h^2 - W - W_1^2\left(\sigma_s^2 - W_2\right)^{-1} \geq 0 \end{cases} \tag{36}$$

and

$$p_{2s}(\gamma_1, \gamma_2) = \frac{1}{2\pi\left(\sigma_s^4 - W_2^2\right)^{\frac{1}{2}}} \times \exp\left[-\frac{\gamma_1^2\sigma_s^2 + \gamma_2^2\sigma_s^2 + 2\gamma_1\gamma_2 W_2}{2\left(\sigma_s^4 - W_2^2\right)}\right]. \tag{37}$$

In the above equations, $W(x)$ is the 1-D height correlation, $W_1(x)$ its first derivative and $W_2(x)$ its second derivative. $\sigma_s^2 = -W_2(0)$ denotes the slope variance.

Moreover

$$L_{12} = \int T^*(w_H, -Q\gamma_1) p_{1s}(\gamma_1) d\gamma_1 \times \exp\left[-Q^2\left(\sigma_h^2 - W - \frac{W_1^2}{2\sigma_s^2}\right) - jQ\frac{\gamma_1 W_1}{\sigma_s^2}\right]. \tag{38}$$

We can note that $L_{12} \equiv L_{12,\alpha\alpha_0}(Q, w_H; x) = L_{12,\alpha\alpha_0}^*(Q, w_H; -x)$ and $L_{22} \equiv L_{22,\alpha\alpha_0}(Q, w_H; x) = L_{22,\alpha\alpha_0}^*(Q, w_H; -x)$ since $W(-x) = W(x), W_1(-x) = -W_1(x)$, and $W_2(-x) = W_2(x)$ (this also holds for a 2-D surface).

For the calculation of $\sigma_{\alpha\alpha_0}^{\mathrm{WCA}Q}$, $\mathbf{v} \equiv v$ is simplified as

$$v(x) = Q\left\{[QW_1(x)]^2 + \sigma_s^2\right\}^{\frac{1}{2}} \quad \text{and} \quad v(\infty) = Q\sigma_s. \tag{39}$$

D. LCA Model

The Local Curvature Approximation (LCA), recently published by Elfouhaily *et al.* [7], [11], [12], can be seen as a generalization of the tilt-invariant approximation [13], [14], valid only for a metallic surface, to the dielectric case. Like WCA, it is reciprocal and converges toward the small perturbation method and the high-frequency Kirchhoff approximation. The Kernel of LCA is very similar of that of SSA. Using the Voronovich notation, it is obtained from the SSA scattering model given by (1) by making the following substitutions

$$\begin{cases} B(\mathbf{k}, \mathbf{k}_0) \to K_E(\mathbf{k}, \mathbf{k}_0)/(2q_k q_0) \\ \hat{M}(\mathbf{k}, \mathbf{k}_0, \mathbf{u}) \to 4Q\hat{T}(\mathbf{k}, \mathbf{k}_0, \mathbf{u})/(2q_k q_0) \end{cases}. \tag{40}$$

Thus, the SPM matrix B is substituted by the Kirchhoff one $K_E/(2q_kq_0)$, where K_E is given from appendices B and C of [7]. Moreover, the kernel $\hat{M}$ is substituted by the kernel $\hat{T}(\mathbf{k},\mathbf{k}_0,\mathbf{u}) \equiv T(\mathbf{w}_H,\mathbf{u})$ given by (21). The scattering cross section of LCA has then the same form as the SSA one expressed from (5). It should be noted that the fact that the SPM matrix is substituted by the Kirchhoff one, implies that the second order term of the NRCS of LCA, $\sigma_{\alpha\alpha_0}^{\mathrm{LCA11}} = \sigma_{\alpha\alpha_0}^{\mathrm{SP}}$, where $\sigma_{\alpha\alpha_0}^{\mathrm{SP}}$ is the NRCS obtained under the stationary phase approximation.

III. Numerical Results in the Backscattering Direction

In this section, the normalized radar cross section (NRCS) is computed for a frequency $f = 14$ GHz (*Ku* band and $\epsilon_r = 47 + j38$ [25]), for a wind speed $u_{10} = 5$ m/s (defined at 10 meters above the sea), in the backscattering direction and for scattering angles $\theta_s \in [0°; 70°]$. In our simulations, we used the Elfouhaily *et al.* [15] omnidirectional sea roughness spectrum, and the sea is assumed to be fully developed (the inverse of the wave age is $\Omega = 0.84$). For a 1-D surface, the NRCS is multiplied by 2π. This is consistent with the NRCS defined as $\sigma(k,k_0) = 2\pi R^2 P/(KL_S|E_0|^2)$, where P is the scattered power, K the incident wave number, L_S the length of the illuminated surface, E_0 the incident field and R the distance from the surface to the receiver.

The advantage to use SSAM, reported in [3], is to compute only a single numerical IFFT [$W_{\alpha\alpha_0}(\mathbf{k},\mathbf{k}_0;\mathbf{r})$, (18)], whereas two numerical IFFT's are needed for SSA [$F_{\alpha\alpha_0}(\mathbf{k},\mathbf{k}_0;\mathbf{r})$ and $G_{\alpha\alpha_0}(\mathbf{k},\mathbf{k}_0;\mathbf{r})$, (13)–(14)]. This computation is made for each scattering angle θ_s, whereas the SSA11 computation requires only one IFFT for the calculation of the height correlation [$W(\mathbf{r})$, (12)], which is independent of θ_s. In addition, to take all the spectral components of $\hat{W}(\mathbf{u})\hat{M}_{\alpha\alpha_0}(\mathbf{k},\mathbf{k}_0;\mathbf{u})$ into account, the upper cut-off wavenumber is chosen equal to 1500 rad/m. This implies a number of samples $N_s = 2^{18} = 262,144$ in order to sample the gravity spectrum with accuracy. For instance, for a wind speed $u_{10} = 5$ m/s, we choose the lower cut-off wavenumber equal to $0.25k_p$ (corresponding to a level of 10^{-5} of the sea gravity normalized spectrum $\hat{W}(u)/\hat{W}_{\max}(u)$, for which $\hat{W}_{\max}(u)$ is obtained for $u = k_p$), where $k_p = \Omega^2 g/u_{10}^2 = 0.2769$ rad/m. This means that the sampling $\Delta u \approx 1500/N_s = 0.005\,72$ rad/m and the number of samples between $0.25k_p$ and k_p is $0.75k_p/\Delta u = 36$, allowing to take into account the gravity with accuracy.

For the simulations, the V and H polarizations are displayed for eight backscattering models:

- SSA11 [(5) with $F_{\alpha\alpha_0} = 0$ and $G_{\alpha\alpha_0} = 0$], full SSA referred to as SSA [SSA11 + SSA12 + SSA22, (5)], SSA used by Voronovich in [3] denoted as SSAM and given by (16);
- full WCA [WCA11 + WCA12 + WCA22, (27)], where the ensemble average is derived from Appendix A, WCA based on the quadratic assumption (32) and referred to as WCAQ;
- full LCA [LCA11 + LCA12 + LCA22, (5) with the substitutions expressed from (40)];
- small perturbation method denoted as SPM ($\sigma_{\alpha\alpha_0}^{\mathrm{SPM}}(k,-k) = |B_{E,\alpha\alpha_0}(k,-k)|^2\hat{W}(2k)$ where $k = K\sin(\theta_s)$, for which K is the incident electromagnetic wave number);
- and the stationary phase approximation referred to as SP (equal to LCA11).

The computing time can be reduced by using the fact that the scattering models (5), (16), (27), and (32) all obey $R^*_{\alpha\alpha_0}(k,k_0;-x) = R_{\alpha\alpha_0}(k,k_0;x) \equiv R(x)$, which means that

$$\int_{-\infty}^{+\infty} e^{-j(k-k_0)x}R(x)\,dx = 2\int_0^{\infty} \Re e\left[e^{-j(k-k_0)x}R(x)\right]dx. \tag{41}$$

Moreover, for the computation of (35), since the integrand $f(\gamma_1,\gamma_2)$ with respect to the surface slopes $\{\gamma_1,\gamma_2\}$ obeys $f^*(-\gamma_1,-\gamma_2) = f(\gamma_1,\gamma_2)$ (it is the case because T is even according to u), we can reduce the computing time by using

$$\int_{-\infty}^{+\infty}\int_{-\infty}^{+\infty} f d\gamma_1 d\gamma_2 = 2\Re e\left[\int_{-\infty}^{+\infty}\int_{0}^{+\infty} f d\gamma_1 d\gamma_2\right]. \tag{42}$$

A. Comparison of SSA11, SP, SPM, and LCA Backscattering Models

In Fig. 1, the NRCS in dB ($10\log_{10}[\sigma_{\alpha\alpha_0}(k,-k)]$ where $k = K\sin\theta_s = -k_s$) of SSA11, SP, SPM, and LCA are displayed versus the scattering angle θ_s, in V (at the top) and H polarizations (at the bottom), for the *Ku* band (frequency $f = 14$ GHz) and for a wind speed $u_{10} = 5$ m/s. We observe that the NRCS decreases more quickly in H polarization as in V polarization. For near-nadir scattering angles, Fig. 1 reveals that the SP, SSA11, and LCA models are similar, which means that SSA11 reproduces the Kirchhoff approximation reduced to the SP approximation (theoretically, SSA11 does not reproduce the Kirchhoff approximation, but since the sea surface is highly conducting and the backscattering angle vanishes, the SPM polarization matrix $B_{E,\alpha\alpha_0}$ is close to the Kirchhoff one $K_{E,\alpha\alpha_0}$). Indeed, for scattering angles ranging from 0° to 20°, only the gravity waves contribute to the scattering and therefore the SP approximation can be applied. However, a smooth transition at scattering angles of 20°–40°, for which the SP model becomes invalid and the Bragg scattering regime (given by the SPM) predominates, is observed. In this region, SSA11 tends toward SPM, whereas the full LCA NRCS goes above SP($\sigma_{\alpha\alpha_0}^{\mathrm{SP}} = \sigma_{\alpha\alpha_0}^{\mathrm{LCA11}}$) and does not converge toward SPM. Thus, although the LCA kernel reaches the small perturbation method and the high-frequency Kirchhoff approximation and it is tilt invariant, the NRCS does not converge toward the Bragg regime. Nevertheless, simulations not reported in this paper, showed for small roughness ($\sigma/\lambda = 0.05$, where SPM is valid) with a Gaussian height spectrum, that the full LCA NRCS converges toward SPM. For a multiscale sea surface, this means that the higher orders of the LCA NRCS ($\sigma_{\alpha\alpha_0}^{\mathrm{LCA12}} + \sigma_{\alpha\alpha_0}^{\mathrm{LCA12}}$) are unable to correct the lowest order ($\sigma_{\alpha\alpha_0}^{\mathrm{LCA11}}$) to converge toward SPM.

For $f = 14$ GHz and $u_{10} = 5$ m/s, the product $K\sigma_h = 48$ where $\sigma_h^2 = 3.95\times10^{-5}u^{4.04}$ [17] is the height variance and $K = 2\pi f/(3\times10^8)$ is the incident electromagnetic wave number. As mentioned by Fung *et al.* [26] (the simulations

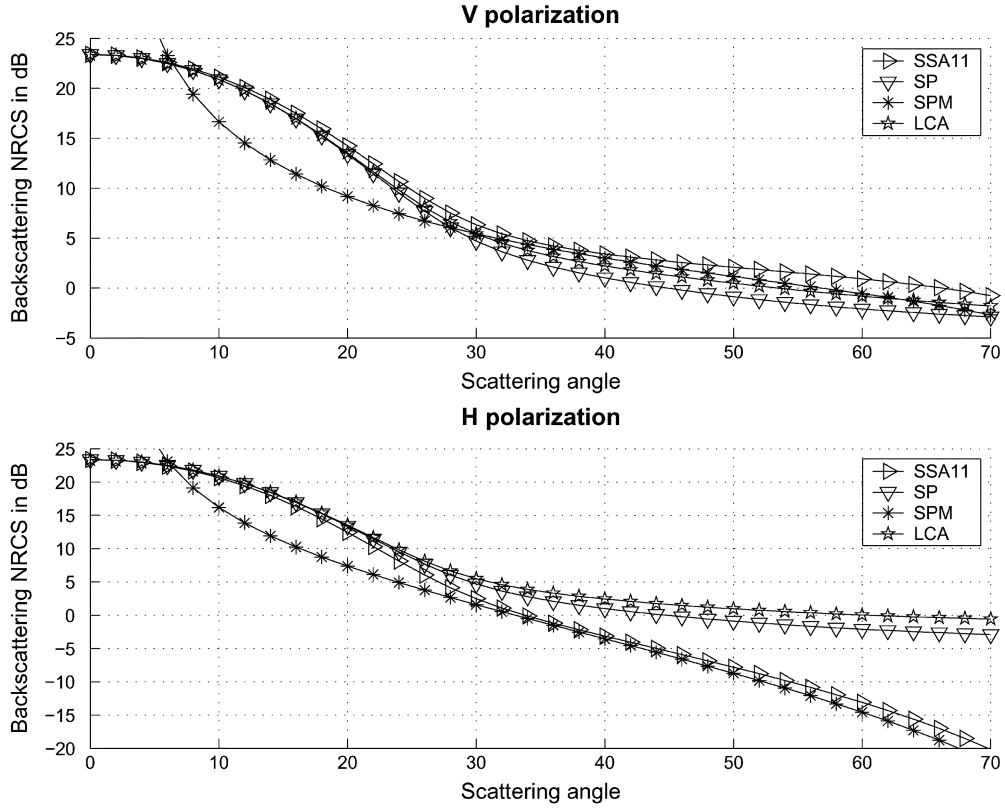

Fig. 1. Comparison of the SSA11, SP, SPM, and LCA backscattering NRCS versus the scattering angle for $f = 14$ GHz and $u_{10} = 5$ m/s and for the V and H polarizations.

are presented for *L* band, $f = 1.6$ GHz), since $K\sigma_h$ is much greater than unity, only a part of the height correlation $W(x)$ is taken into account for the integration over x of $R^{\mathrm{SSA11}}(x)$. In addition, although the difference between the height correlation computed from the gravity spectrum $[W_G(x)]$ and the full spectrum $[W_F(x)$ gravity plus capillarity] is small, the contribution of the capillary waves related to the high frequency spectrum must be taken into account with accuracy. Indeed, for $K\sigma_h > 1$, if the difference $W_F(x) - W_G(x)$ is small, then the difference $Q^2[W_F(x) - W_G(x)]\,(Q = 2K\sigma_h \cos\theta_s)$ can become significative. Thus, the difference $e^{-Q^2[1-W_F(x)/\sigma_h^2]} - e^{-Q^2[1-W_G(x)/\sigma_h^2]}$ become significative, implying that the corresponding R^{SSA11} are very different. In conclusion, in the computation of the height correlation, all spectral components of the height spectrum must be included to reproduce the Bragg regime, which occurs for moderate scattering angles.

B. Comparison of SSA11, SSA11 + SSA12, SSA, and SSAM

In Fig. 2, the same variation as Fig. 1 is plotted for the SSA11, SSA11 + SSA12, SSA, and SSAM backscattering NRCS. In addition, in Fig. 3, the backscattering NRCS $\sigma^{\mathrm{SSA}}/\sigma^{\mathrm{SSA11}}, \sigma^{\mathrm{SSA}}/(\sigma^{\mathrm{SSA11}} + \sigma^{\mathrm{SSA12}})$ and $\sigma^{\mathrm{SSA}}/\sigma^{\mathrm{SSAM}}$ are plotted versus the scattering angle in dB scale. For the V polarization and scattering angles $\theta_s \in [0°; 30°]$, all NRCS are similar within 1 dB whereas for the H polarization, the NRCS all similar up to 20°. Above this lower limit, SSA11 goes below SSA and their deviation increases with the scattering angle and it is stronger for the H polarization. As expected, the contributions of the higher order terms (SSA12 and SSA22) increase with the scattering angle. SSAM follows SSA11 up to 40°–50° and above this angle is converged toward SSA but without reaching it. The accuracy of SSA11 depends not only on the rms slope, but also on the polarization. The reason [3], [6] for the different behavior of the two polarizations is the stronger dependency of the backscattering NRCS on the incidence angle for the H polarization, which leads to more pronounced modulation effects as compared to the V polarization case. Indeed, in *Ku* band, for a 2-D sea surface, for wind speeds $u_{10} = \{5, 15\}$ m/s, for scattering angles $\theta_s \in [0°; 60°]$, and for the V and H polarizations, a comparison of SSA11 and SSAM with TSM was used in paper [3]. This allowed the author of paper [6] to conclude that SSAM takes into account the tilt modulation of the Bragg scattering by the large-scale surface components, whereas the SSA11 does not. In addition, he noticed for the H-polarization that the difference between the TSM and the SSA11 results practically disappears when the SSAM contribution is added. On the other hand, for the V polarization, this difference was already negligible and therefore SSAM provides a very small correction.

C. Comparison of WCA11, WCA11 + WCA12, WCA and WCAQ

In Fig. 4, the same variation as Fig. 1 is plotted for the $\mathrm{WCA11}, \mathrm{WCA11} + \mathrm{WCA12}, \mathrm{WCA}$ and WCAQ backscattering NRCS. In addition, in Fig. 5, the backscattering NRCS $\sigma^{\mathrm{WCA}}/\sigma^{\mathrm{WCA11}}, \sigma^{\mathrm{WCA}}/(\sigma^{\mathrm{WCA11}} + \sigma^{\mathrm{WCA12}})$ and $\sigma^{\mathrm{WCA}}/\sigma^{\mathrm{WCAQ}}$ are plotted versus the scattering angle in dB

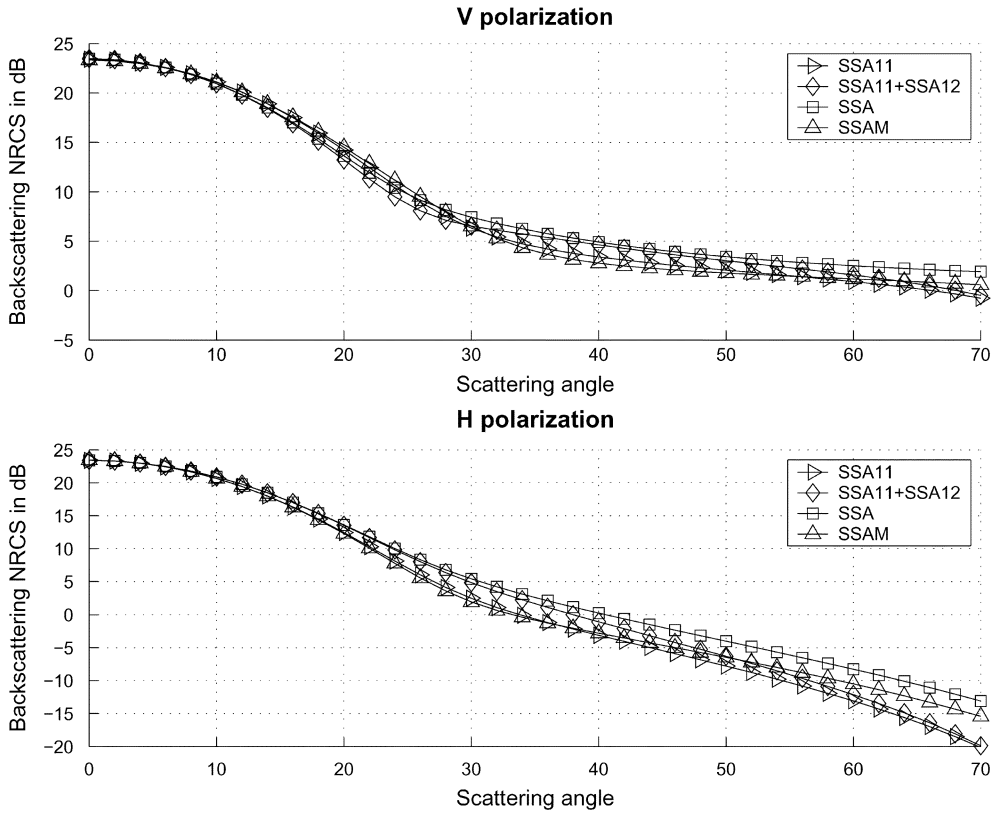

Fig. 2. Same variation as Fig. 1 for the $\mathrm{SSA11}, \mathrm{SSA11} + \mathrm{SSA12}, \mathrm{SSA}$ and SSAM backscattering NRCS.

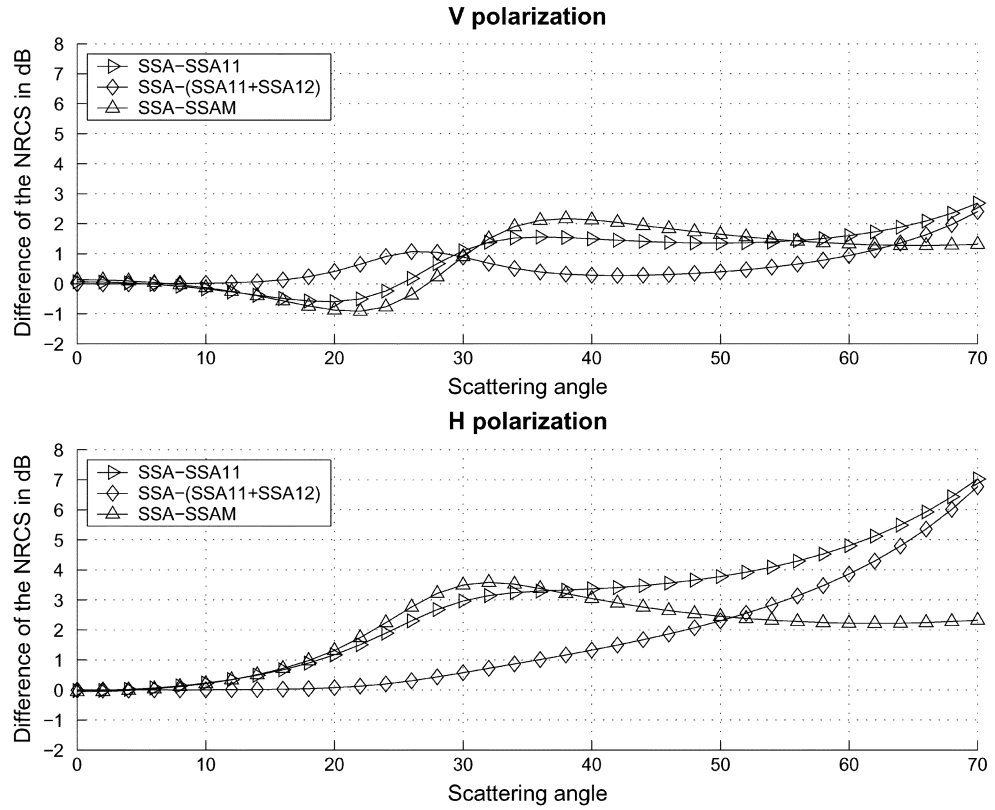

Fig. 3. Backscattering NRCS $10\log(\sigma^{\mathrm{SSA}}/\sigma^{\mathrm{SSA11}}), 10\log[\sigma^{\mathrm{SSA}}/(\sigma^{\mathrm{SSA11}} + \sigma^{\mathrm{SSA12}})]$ and $10\log(\sigma^{\mathrm{SSA}}/\sigma^{\mathrm{SSAM}})$, where $\sigma^{\mathrm{SSA}} = \sigma^{\mathrm{SSA11}} + \sigma^{\mathrm{SSA12}} + \sigma^{\mathrm{SSA22}}$ versus the scattering angle.

scale. We observe that WCAQ can not reach WCA. This may be explained by the fact that the ensemble average of WCA involves the height correlation $W(\mathbf{r})$ and its first $\boldsymbol{\nabla} W(\mathbf{r})$ and second $\boldsymbol{\nabla}\boldsymbol{\nabla} W(\mathbf{r})$ derivatives, whereas WCAQ uses only

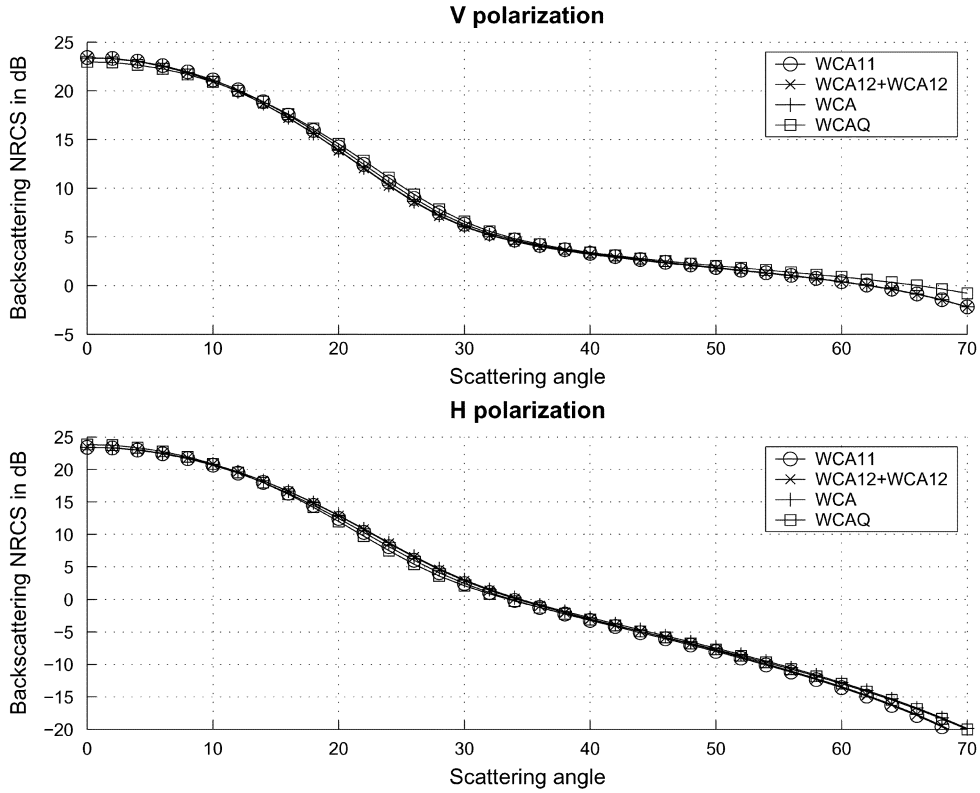

Fig. 4. Same variation as Fig. 1 for the WCA11, WCA11 + WCA12, WCA, and WCAM backscattering NRCS.

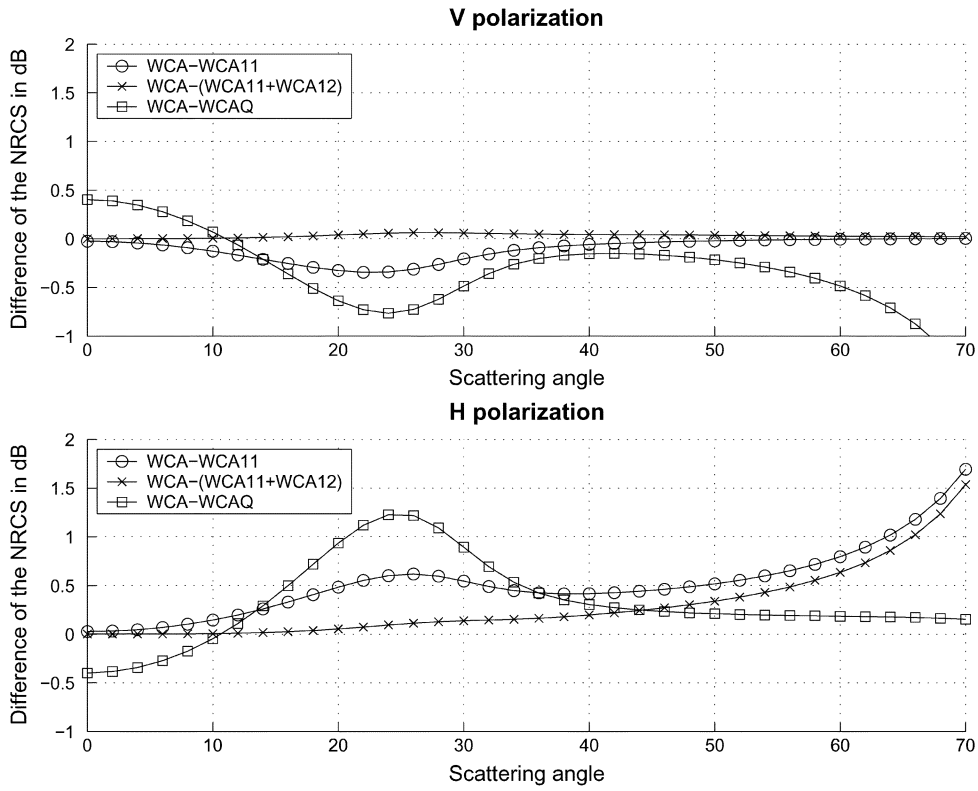

Fig. 5. Backscattering NRCS $10\log(\sigma^{\mathrm{WCA}}/\sigma^{\mathrm{WCA11}})$, $10\log[\sigma^{\mathrm{WCA}}/(\sigma^{\mathrm{WCA11}}+\sigma^{\mathrm{WCA12}})]$, and $10\log(\sigma^{\mathrm{WCA}}/\sigma^{\mathrm{WCAQ}})$, where $\sigma^{\mathrm{WCA}}=\sigma^{\mathrm{WCA11}}+\sigma^{\mathrm{WCA12}}+\sigma^{\mathrm{WCA22}}$ versus the scattering angle.

$W(\mathbf{r})$ and $\boldsymbol{\nabla}W(\mathbf{r})$. Indeed, $\boldsymbol{\nabla}\boldsymbol{\nabla}W(\mathbf{r})$ is related to the surface slope correlation. For the V polarization, WCA is weakly below of WCA11 ($\sigma_V^{\mathrm{WCA}}-\sigma_V^{\mathrm{WCA11}}\leq 0$) whereas for the H polarization, the opposite effect is observed. Thus, for the V polarization, the contributions of the higher order terms (WCA12 and WCA22) are negative. In fact, Fig. 5 reveals

TABLE I
VALUES OF $\max|\sigma^{\mathrm{WCA}}_{\alpha\alpha_0}/\sigma^{\mathrm{WCA11}}_{\alpha\alpha_0}|$ AND $\max|\sigma^{\mathrm{SSA}}_{\alpha\alpha_0}/\sigma^{\mathrm{SSA11}}_{\alpha\alpha_0}|$ IN dB SCALE, WHERE $\sigma^{\mathrm{SSA11}}_{\alpha\alpha_0} = \sigma^{\mathrm{WCA11}}_{\alpha\alpha_0}$, ACCORDING TO THE WIND SPEED u_{10}, THE FREQUENCY f AND FOR $\theta_s \in [0; 70]$ DEGREES

	5 m/s, 5.3 GHz	15 m/s, 5.3 GHz	5 m/s, 14 GHz	15 m/s, 14 GHz
$\max\|\sigma_V^{WCA}/\sigma_V^{WCA11}\|$	0.3 dB	0.4 dB	0.4 dB	0.5 dB
$\max\|\sigma_V^{SSA}/\sigma_V^{SSA11}\|$	3.7 dB	4.3 dB	2.7 dB	3.6 dB
$\max\|\sigma_H^{WCA}/\sigma_H^{WCA11}\|$	1.1 dB	2.1 dB	1.7 dB	5.5 dB
$\max\|\sigma_H^{SSA}/\sigma_H^{SSA11}\|$	8.4 dB	9.3 dB	7.0 dB	9.5 dB

for the V polarization that $\sigma_V^{\mathrm{WCA12}} \leq 0$ and $\sigma_V^{\mathrm{WCA22}} \geq 0$ with $|\sigma_V^{\mathrm{WCA12}}| \gg \sigma_V^{\mathrm{WCA22}}$, whereas for the H polarization, $\sigma_H^{\mathrm{WCA12}} \geq 0$ and $\sigma_H^{\mathrm{WCA22}} \geq 0$. As the SSA model, the contributions of the higher order terms are larger for the H polarization and increase with the scattering angle. Nevertheless for WCA, the difference between the second order (σ^{WCA11}) and its higher order terms is smaller than that SSA (comparison of Fig. 3 with Fig. 5, where $\sigma^{\mathrm{SSA11}} = \sigma^{\mathrm{WCA11}}$). Therefore, the large-scale tilt-modulation predicted by WCA is smaller than that obtained for SSA.

IV. CONCLUSION

In this paper, the NRCS of the WCA, LCA and the first- [SSA(1)] and second- [SSA(2)] order SSA are compared. The sea surface is assumed to be 1-D with Gaussian statistics and the Elfouhaily *et al.* elevation omnidirectional spectrum is considered. To study the assumption used by Voronovich *et al.* [3] to include the SSA(2) contribution, the SSAM is also computed. This model has the advantage to demand the computation of two IFFT's instead of three for SSA. In addition, the second-order statistical moment of WCA is calculated rigorously for any 2-D height correlation by assuming Gaussian statistics. To reduce the number of the numerical integrations of WCA, a quadratic assumption on the kernel of the WCA scattered field is proposed to derive the NRCS, denoted as WCAQ. For a wind speed $u_{10} = 5$ m/s and a frequency $f = 14$ GHz, this paper displays the backscattering NRCS of these scattering models versus the scattering angle $\theta_s \in [0°; 70°]$.

For near-nadir scattering angles, numerical results show that SSA11 (second order of the SSA NRCS), SSAM, LCA11 (second order of the LCA NRCS, $\sigma^{\mathrm{LCA11}} = \sigma^{\mathrm{SP}}$ where σ^{SP} is the Kirchhoff approximation reduced to the stationary phase) are similar and WCAQ differs from these models of 0.5 dB. Moreover, the contributions of the higher order terms of SSA, WCA and LCA are negligible. For scattering angles greater than 20°–30° where the large-wave tilt modulation occurs, SSA11 converges toward small perturbation method (SPM) and the contributions of the higher order terms increase with the scattering angle and it is greater for the H polarization than the V polarization. We can observe that SSAM underestimates SSA within 2–3 dB and the modulation effects predicted by WCA are smaller than the SSA ones. A possible explanation is that the SSA scattered field kernel $\hat{M}$, verifies $\nabla\hat{M}|_{\mathbf{u}=\mathbf{0}} = \mathbf{0}$, whereas $\nabla\hat{T}|_{\mathbf{u}=\mathbf{0}} = \mathbf{0}$, for the WCA model. Indeed the modulation effects are related to the derivatives of $\hat{M}$ and $\hat{T}$. For any polarization, the full SSA NRCS is larger than its lower order, whereas for the WCA model in V polarization, the opposite effect is observed. Elfouhaily *et al.* [7] noted the same effect with a Gaussian spectrum.

Although the LCA scattered field kernel converges toward SPM for small roughness, its backscattering NRCS does not converge toward SPM for a multiscale sea surface. This deficiency can be explained as follows. In [6], Voronovich showed that the modulation effects are taken into account with a first-order accuracy on a (dimensionless) if (43), holds [(23) of [6] simplified for a 1-D surface in the backscattering direction]

$$\begin{aligned}\frac{(q_k+ak)^2}{q_k^2}B(k-aq_k,-[k-aq_k]) &= B(k,-k) - \frac{1}{4}\frac{d\hat{M}(k,-k;u))}{du}\Big|_{u=0} \\ &\quad - \frac{\hat{M}(k,-k;2k-2aq_k))}{8q_k} + \mathcal{O}(a^2). \end{aligned} \tag{43}$$

For $a = 0$, equality (43) holds for the SSA model because $\hat{M}(\mathbf{k},\mathbf{k}_0;\mathbf{k}-\mathbf{k}_0-\mathbf{u}) = \hat{M}(\mathbf{k},\mathbf{k}_0;\mathbf{u})$ and $\hat{M}(\mathbf{k},\mathbf{k}_0;\mathbf{0}) = 0$. For the LCA model, $\hat{M}(k,-k;u) \to 4\hat{T}(k,-k;u)/q_k$ and $B(-k,k) \to K_E(-k,k)/(2q_k^2)$ are substituted from (40). In addition, since $\hat{T}(k,-k;u)$ is quadratic in its lower order, we have $d\hat{T}(k,-k;u)/du|_{u=0} = 0$. Thus, for $a = 0$, equality (43) becomes for the LCA model, $K_E(k,-k) = K_E(k,-k) - \hat{T}(k,-k;2k) = K_E(k,-k) - 2k^2$ for a perfectly conducting surface ($\hat{T}(k,-k;u) = u^2/2$). This equality holds if $k = 0$. It is not the case. Hence, the general property, $\hat{M}(\mathbf{k},\mathbf{k}_0;\mathbf{k}-\mathbf{k}_0-\mathbf{u}) = \hat{M}(\mathbf{k},\mathbf{k}_0;\mathbf{u})$, of the scattered field kernel, seems to be fundamental to obtain the modulation effects.

Simulations not reported in this paper, showed for a greater wind speed ($u_{10} = 15$ m/s) and for a lower frequency ($f = 5.3$ GHz), that the differences between SSA11-SSA and WCA11-WCA increase with the wind speed and varies weakly with the frequency (see Table I).

Numerically, for a 1-D surface, WCA requires two fold numerical integrations over the surface slopes, whereas SSA requires the computation of two 1-D IFFT's. Nevertheless, for SSA, the number of samples to calculate the IFFT is $N_s = 2^{18} = 262,144$, whereas for WCA, we use $N_s \times N_s = 80 \times 80$. The calculations of the height correlation and its derivatives are not accounted for because they have been computed before and were saved in a data file. The integration over x is not taken into account because it is shared by WCA and SSA. WCAQ can be simulated easily since it demands only two-fold integrations, whereas WCA requires two additional two fold integrations.

For a 2-D problem, the simulation of SSA becomes a very difficult task due to the number of samples required for the calculation of the two bi-dimensional IFFT's. This is why

Voronovich *et al.* [3] used the approximate model SSAM and evaluated the IFFT with an another method by considering the spectrum on logarithmic scale. Monte Carlo methods for evaluating the WCA and the SSA NRCS could be used. These may be more computationally efficient for some cases (from linear and nonlinear ocean surface realizations) than computing the multidimensional integrals. Comparison with benchmark numerical methods [9], [21], [22], [27]–[29] (see also the papers quoted in these references) would permit to study the validity of these asymptotic backscattering models. However, for a sea surface, the SSA model seems to be better than the WCA model because the modulation effects predicted by WCA are very small. Numerical simulations would resolve this issue.

APPENDIX A

This Appendix is devoted to the calculation of the ensemble averages (23)–(25) for a surface slope and elevation joint Gaussian process and for any 2-D anisotropic correlation function. To facilitate the notation, the subscripts are omitted. Only the expected values over the elevations h_1 and h_2 are derived since $T(\mathbf{w}_H, \mathbf{u})$ is a complicated function of $\mathbf{u}$.

Firstly, $\langle T^*(\mathbf{w}_H, -Q\boldsymbol{\nabla}h_2)T(\mathbf{w}_H, -Q\boldsymbol{\nabla}h_1)e^{jQ(h_2-h_1)}\rangle$ is calculated. The covariance matrix of the random variables $\{h_1, h_2, \boldsymbol{\nabla}h_1\boldsymbol{\nabla}h_2\} \equiv \{h_1, h_2, \gamma_{1x}, \gamma_{2x}, \gamma_{1y}, \gamma_{2y}\}$ has to be known. $\{\gamma_{1x}, \gamma_{2x}\}$ denote the surface slopes along the direction $\hat{\mathbf{x}}$ at the points 1 and 2, respectively, whereas $\{\gamma_{1y}, \gamma_{2y}\}$ stand for the surface slopes along the $\hat{\mathbf{y}}$ direction at the points 1 and 2, respectively. This covariance matrix is given by (25) of [30]. Moreover, we can note that the operator $\mathcal{L}(\cdots)$ given by (26) depends on the elevation difference $h = h_2 - h_1$. Thus, h defined as the difference of Gaussian variables is also Gaussian. Thus from (25) of [30], we show that the covariance matrix of $\{h, \gamma_{1x}, \gamma_{2x}, \gamma_{1y}, \gamma_{2y}\}$ is

$$[C_5] = \begin{bmatrix} W_h & -W_{1x} & -W_{1x} & -W_{1y} & -W_{1y} \\ -W_{1x} & \sigma_{sx}^2 & -W_{2x} & 0 & -W_{2xy} \\ -W_{1x} & -W_{2x} & \sigma_{sx}^2 & -W_{2xy} & 0 \\ -W_{1y} & 0 & -W_{2xy} & \sigma_{sy}^2 & -W_{2y} \\ -W_{1y} & -W_{2xy} & 0 & -W_{2y} & \sigma_{sy}^2 \end{bmatrix} \tag{A1}$$

where $W_h = 2(\sigma_h^2 - W), W_{1x} = \partial_{1,0}W, W_{1y} = \partial_{0,1}W, W_{2x} = \partial_{2,0}W, W_{2y} = \partial_{0,2}W, W_{2xy} = \partial_{1,1}W$, in which $\partial_{n,m} = \partial^{n+m}/(\partial x^n \partial y^m)$. $W(\mathbf{r}) = W(x, y)$ is the surface height correlation function in Cartesian coordinates (x, y). $W(\mathbf{0}) = \sigma_h^2$ is the height variance and $-W_{2x}(\mathbf{0}) = \sigma_{sx}^2, -W_{2y}(\mathbf{0}) = \sigma_{sy}^2$ are the slope variances in the up- and cross-directions, respectively. To have a real surface without imaginary part, its spectrum has to be Hermitian, which implies that the correlation function $\mathrm{W}(\mathbf{r})$ is even with respect to the two directions $\{\hat{\mathbf{x}}, \hat{\mathbf{y}}\}$. This implies that $W_{1x}(\mathbf{0}) = 0, W_{1y}(\mathbf{0}) = 0$, and $W_{2xy}(\mathbf{0}) = 0$. The ensemble average L_{22} is defined as

$$L_{22} = \int\int T^*(\mathbf{w}_H, -Q\boldsymbol{\nabla}h_2)T(\mathbf{w}_H, -Q\boldsymbol{\nabla}h_1) \times \left[\int_{-\infty}^{+\infty} p_5(h, \boldsymbol{\nabla}h_1, \boldsymbol{\nabla}h_2)e^{jQh}dh\right] d\boldsymbol{\nabla}h_1 d\boldsymbol{\nabla}h_2 \tag{A2}$$

where

$$p_5(h, \boldsymbol{\nabla}h_1, \boldsymbol{\nabla}h_2) = \frac{1}{(2\pi)^{\frac{5}{2}}|[C_5]|^{\frac{1}{2}}} \exp\left(-\frac{\mathbf{V}_5^T[C_5]^{-1}\mathbf{V}_5}{2}\right) \tag{A3}$$

in which $\mathbf{V}_5^T = [h\ \gamma_{1x}\ \gamma_{2x}\ \gamma_{1y}\ \gamma_{2y}] \equiv [h\,\boldsymbol{\nabla}h_1\ \boldsymbol{\nabla}h_2]$. The superscript T stands for transpose ($\mathbf{V}_5$ is a column vector of length 5). To inverse the matrix $[C_5], [C_5]$ is partitioned as

$$[C_5] = \begin{bmatrix} W_h & \mathbf{Y}_4^T \\ \mathbf{Y}_4 & [C_4] \end{bmatrix} \tag{A4}$$

where

$$\mathbf{Y}_4 = \begin{bmatrix} -W_{1x} \\ -W_{1x} \\ -W_{1y} \\ -W_{1y} \end{bmatrix}$$

$$[C_4] = \begin{bmatrix} \sigma_{sx}^2 & -W_{2x} & 0 & -W_{2xy} \\ -W_{2x} & \sigma_{sx}^2 & -W_{2xy} & 0 \\ 0 & -W_{2xy} & \sigma_{sy}^2 & -W_{2y} \\ -W_{2xy} & 0 & -W_{2y} & \sigma_{sy}^2 \end{bmatrix}. \tag{A5}$$

In addition from [31], we have

$$[C_5]^{-1} = \begin{bmatrix} H & \mathbf{X}_4^T \\ \mathbf{X}_4 & [G] \end{bmatrix} \tag{A6}$$

where

$$H = \left(W_h - \mathbf{Y}_4^T[C_4]^{-1}\mathbf{Y}_4\right)^{-1}, \tag{A7}$$

$$\mathbf{X}_4 = -H[C_4]^{-1}\mathbf{Y}_4, \tag{A8}$$

$$[G] = [C_4]^{-1} + H([C_4]^{-1}\mathbf{Y}_4)\left(\mathbf{Y}_4^T[C_4]\right)^{-1} \tag{A9}$$

$$|[C_5]| = |[C_4]|/H \tag{A10}$$

in which, H is a scalar, $\mathbf{X}_4$ a column vector of length four, $[G]$ a square matrix of length 4, $|[C_5]|$ the determinant of $[C_5]$ expressed from the determinant of $[C_4]$ denoted as $|[C_4]|$. The substitution of (A6) and (A10) into (A3) yields

$$p_5(h, \boldsymbol{\nabla}h_1, \boldsymbol{\nabla}h_2) = \frac{1}{(2\pi)^{\frac{5}{2}}}\left(\frac{H}{|[C_4]|}\right)^{\frac{1}{2}} \exp\left(-\frac{\mathbf{V}_4^T[G]\mathbf{V}_4 + h^2H + 2h\mathbf{V}_4^T \cdot \mathbf{X}_4}{2}\right) \tag{A11}$$

where $\mathbf{V}_4^T = [\gamma_{1x}\ \gamma_{2x}\ \gamma_{1y}\ \gamma_{2y}] \equiv [\boldsymbol{\nabla}h_1\ \boldsymbol{\nabla}h_2]$, which is independent of h. Therefore, using

$$\int_{-\infty}^{\infty} \exp(-a_4x^2 - 2b_4x - c_4) = \left(\frac{\pi}{a_4}\right)^{\frac{1}{2}} \exp\left(\frac{b_4^2}{a_4} - c_4\right) \tag{A12}$$

where $a_4 > 0$ and setting $a_4 = H/2, b_4 = (\mathbf{V}_4^T \cdot \mathbf{X}_4 - jQ)/2, c_4 = \mathbf{V}_4^T[G]\mathbf{V}_4/2$, the substitution of (A12) into (A2) leads to

$$L_{22} = \frac{1}{(2\pi)^2|[C_4]|^{\frac{1}{2}}} \int\int T^*(\mathbf{w}_H, -Q\boldsymbol{\nabla}h_2) \times T(\mathbf{w}_H, -Q\boldsymbol{\nabla}h_1) \exp\left(\frac{b_4^2}{a_4} - c_4\right) d\boldsymbol{\nabla}h_1 d\boldsymbol{\nabla}h_2. \tag{A13}$$

In addition, from (A8)–(A9) we get $b_4 = -a_4\alpha_4 - jQ/2, c_4 = (\mathbf{V}_4^T[C_4]^{-1}\mathbf{V}_4)/2 + a_4\alpha_4^2$, where $\alpha_4 = \mathbf{V}_4^T[C_4]^{-1}\mathbf{Y}_4$. Thus, the above equation becomes

$$L_{22} = \int\int T^*(\mathbf{w}_H, -Q\boldsymbol{\nabla}h_2)T(\mathbf{w}_H, -Q\boldsymbol{\nabla}h_1) \times \exp\left(-\frac{Q^2}{4a_4} + jQ\alpha_4\right) p_{s4}(\boldsymbol{\nabla}h_1, \boldsymbol{\nabla}h_2)d\boldsymbol{\nabla}h_1 d\boldsymbol{\nabla}h_2 \quad \text{(A14)}$$

where

$$p_{s4}(\boldsymbol{\nabla}h_1, \boldsymbol{\nabla}h_2) = \frac{1}{(2\pi)^2|[C_4]|^{\frac{1}{2}}} \exp\left(-\frac{\mathbf{V}_4^T[C_4]^{-1}\mathbf{V}_4}{2}\right) \quad \text{(A15)}$$

and $(4a)^{-1}, \alpha_4$ are given in (A16) and (A17), shown at the bottom of the page. In (A15), the subscript s indicates that the joint probability density function p_{s4} of dimension 4 is over the surface slopes. We can note that L_{22} demands the calculation of $[C_4]^{-1}$, which can be derived analytically. If $W_{1x} = W_{1y} = 0$ (the correlation between the elevations and the slopes is neglected), then $\alpha_4 = 0, (4a)^{-1} = \sigma_h^2 - W, \exp[-Q^2(4a)^{-1} + jQ\alpha_4] = \exp[-Q^2(\sigma_h^2 - W)]$ which is equal to the characteristic function of the random variable $Q(h_2 - h_1)$.

The contribution of the coherent term $L_{22}^{\infty} = |\langle T(\mathbf{w}_H, -Q\boldsymbol{\nabla}h_1)\exp(-jQh_1)\rangle|^2$, related to $|\langle S_2(\mathbf{k}, \mathbf{k}_0)\rangle|^2$, is obtained from (A14) by omitting the correlation ($r \to \infty$). This means from (A5) that $\mathbf{Y}_4 = \mathbf{0}$ and that the matrix $[C_4]$ becomes diagonal. Thus, from (A16) and (A17), $\alpha_4 = 0, (4a)^{-1} = \sigma_h^2$, and we have

$$L_{22}^{\infty} = e^{-Q^2\sigma_h^2}|\int T(\mathbf{w}_H, -Q\boldsymbol{\nabla}h_1)p_{s2}(\boldsymbol{\nabla}h_1)d\boldsymbol{\nabla}h_1|^2. \quad \text{(A18)}$$

From (A14), it is easy to calculate $L_{12} = \langle T^*(\mathbf{w}_H, -Q\boldsymbol{\nabla}h_2)\exp[jQ(h_2 - h_1)]\rangle$ giving

$$L_{12} = \int T^*(\mathbf{w}_H, -Q\boldsymbol{\nabla}h_2)e^{-\frac{Q^2}{4a_2} + jQ\alpha_2}p_{s2}(\boldsymbol{\nabla}h_2)d\boldsymbol{\nabla}h_2 \quad \text{(A19)}$$

where

$$\frac{1}{4a_2} = \sigma_h^2 - W - \frac{1}{2}\left(\frac{W_{1x}^2}{\sigma_{sx}^2} + \frac{W_{1y}^2}{\sigma_{sy}^2}\right), \quad \text{(A20)}$$

$$\alpha_2 = -\left(\frac{W_{1x}\gamma_{2x}}{\sigma_{sx}^2} + \frac{W_{1y}\gamma_{2y}}{\sigma_{sy}^2}\right). \quad \text{(A21)}$$

$$p_{s2}(\boldsymbol{\nabla}h_2) = \frac{1}{2\pi\sigma_{sx}\sigma_{sy}} \exp\left(-\frac{\gamma_{2x}^2}{2\sigma_{sx}^2} - \frac{\gamma_{2y}^2}{2\sigma_{sy}^2}\right). \quad \text{(A22)}$$

As previously said, the contribution of the coherent term $L_{12}^{\infty} = \langle\exp(-jQh_1)\rangle\langle T^*(\mathbf{w}_H, -Q\boldsymbol{\nabla}h_2)\exp(-jQh_2)\rangle$, related to $\langle S_1(\mathbf{k}, \mathbf{k}_0)\rangle\langle S_2^*(\mathbf{k}, \mathbf{k}_0)\rangle$, can be easily derived from (A19) by omitting the correlation. This yields

$$L_{12}^{\infty} = e^{-Q^2\sigma_h^2}\int T^*(\mathbf{w}_H, -Q\boldsymbol{\nabla}h_2)p_{s2}(\boldsymbol{\nabla}h_2)d\boldsymbol{\nabla}h_2. \quad \text{(A23)}$$

APPENDIX B

The general expressions for kernel functions $B_{\alpha\alpha_0}$ and $\hat{B}_{2,\alpha\alpha_0}$ on the basis of vertically and horizontally polarized waves are given in [3] and are as follows. The first order is

$$B_{11}(\mathbf{k}, \mathbf{k}_0) = \frac{(\epsilon_r - 1)\left(q_k'q_0'\frac{\mathbf{k}\cdot\mathbf{k}_0}{kk_0} - \epsilon_r kk_0\right)}{(\epsilon_r q_k + q_k')(\epsilon_r q_0 + q_0')} \quad \text{(B1)}$$

$$B_{12}(\mathbf{k}, \mathbf{k}_0) = \frac{(\epsilon_r - 1)Kq_k'\mathbf{N}\cdot(\mathbf{k}\times\mathbf{k}_0)}{(\epsilon_r q_k + q_k')(q_0 + q_0')kk_0} \quad \text{(B2)}$$

$$B_{21}(\mathbf{k}, \mathbf{k}_0) = \frac{(\epsilon_r - 1)Kq_0'\mathbf{N}\cdot(\mathbf{k}\times\mathbf{k}_0)}{(q_k + q_k')(\epsilon_r q_0 + q_0')kk_0} \quad \text{(B3)}$$

$$B_{22}(\mathbf{k}, \mathbf{k}_0) = -\frac{(\epsilon_r - 1)K^2\mathbf{k}\cdot\mathbf{k}_0}{(q_k + q_k')(q_0 + q_0')kk_0}. \quad \text{(B4)}$$

The second order are expressed from (B5) as follows:

$$\begin{aligned}\hat{B}_{2,11}(\mathbf{k}, \mathbf{k}_0; \mathbf{u}) &= \frac{(\epsilon_r - 1)}{(\epsilon_r q_k + q_k')(\epsilon_r q_0 + q_0')} \\ &\times \left[-2\frac{\epsilon_r - 1}{\epsilon_r q_u + q_u'}\left(q_k'q_0'\frac{\mathbf{k}\cdot\mathbf{u}}{k}\frac{\mathbf{k}_0\cdot\mathbf{u}}{k_0} + \epsilon_r kk_0u^2\right)\right. \\ &+ 2\epsilon_r\frac{q_u + q_u'}{\epsilon_r q_u + q_u'}\left(k_0q_k'\frac{\mathbf{k}\cdot\mathbf{u}}{k} + kq_0'\frac{\mathbf{k}_0\cdot\mathbf{u}}{k_0}\right) \\ &\left. - (\epsilon_r K^2(q_k' + q_0') + 2q_k'q_0'(q_u - q_u'))\frac{\mathbf{k}\cdot\mathbf{k}_0}{kk_0}\right],\end{aligned}$$

$$\begin{aligned}\hat{B}_{2,12}(\mathbf{k}, \mathbf{k}_0; \mathbf{u}) &= \frac{(\epsilon_r - 1)K}{(\epsilon_r q_k + q_k')(q_0 + q_0')}\left[\frac{\mathbf{N}\cdot(\mathbf{u}\times\mathbf{k}_0)}{k_0(\epsilon_r q_u + q_u')}\right. \\ &\times \left(-2(\epsilon_r - 1)q_k'\frac{\mathbf{k}\cdot\mathbf{u}}{k} + 2\epsilon_r(q_u + q_u')k\right) \\ &\left. - \frac{\mathbf{N}\cdot(\mathbf{k}\times\mathbf{k}_0)}{kk_0}(\epsilon_r K^2 + q_k'q_0' + 2q_k'(q_u - q_u'))\right],\end{aligned}$$

$$\frac{1}{4a} = \frac{1}{2H} = \sigma_h^2 - W - \frac{W_{1y}^2\left(\sigma_{sx}^2 - W_{2x}\right) + W_{1x}^2\left(\sigma_{sy}^2 - W_{2y}\right) + 2W_{1x}W_{1y}W_{2xy}}{\sigma_{sx}^2\sigma_{sy}^2 + W_{2x}W_{2y} - \sigma_{sx}^2W_{2y} - \sigma_{sy}^2W_{2x} + W_{2xy}^2} \quad \text{(A16)}$$

$$\alpha_4 = \frac{\left[W_{1x}\left(W_{2y} - \sigma_{sy}^2\right) - W_{1y}W_{2xy}\right](\gamma_{1x} + \gamma_{2x}) + \left[W_{1y}\left(W_{2x} - \sigma_{sx}^2\right) - W_{1x}W_{2xy}\right](\gamma_{1y} + \gamma_{2y})}{\sigma_{sx}^2\sigma_{sy}^2 + W_{2x}W_{2y} - \sigma_{sx}^2W_{2y} - \sigma_{sy}^2W_{2x} + W_{2xy}^2} \quad \text{(A17)}$$

$$\hat{B}_{2,21}(\mathbf{k},\mathbf{k}_0;\mathbf{u}) = \frac{(\epsilon_r-1)K}{(q_k+q_k')(\epsilon_r q_0+q_0')}\left[\frac{\mathbf{N}\cdot(\mathbf{u}\times\mathbf{k})}{k(\epsilon_r q_u+q_u')}\times\left(2(\epsilon_r-1)q_0'\frac{\mathbf{k}_0\cdot\mathbf{u}}{k_0}-2\epsilon_r(q_u+q_u')k_0\right)-\frac{\mathbf{N}\cdot(\mathbf{k}\times\mathbf{k}_0)}{kk_0}(\epsilon_r K^2+q_k'q_0'+2q_0'(q_u-q_u'))\right]$$

$$\hat{B}_{2,22}(\mathbf{k},\mathbf{k}_0;\mathbf{u}) = \frac{(\epsilon_r-1)K^2}{(q_k+q_k')(q_0+q_0')}\left[-2\frac{\epsilon_r-1}{\epsilon_r q_u+q_u'}\times\left(\frac{\mathbf{k}\cdot\mathbf{u}}{k}\frac{\mathbf{k}_0\cdot\mathbf{u}}{k_0}-u^2\frac{\mathbf{k}\cdot\mathbf{k}_0}{kk_0}\right)+\left(q_k'+q_0'+2(q_u-q_u')\frac{\mathbf{k}\cdot\mathbf{k}_0}{kk_0}\right)\right]. \quad \text{(B5)}$$

Here, $\{-q_0, q_k\}$ and $\{-q_0', q_k'\}$ are the vertical components of the appropriate wavevectors in the first (air) and the second (dielectric) media

$$q_k=(K^2-\mathbf{k}^2)^{\frac{1}{2}},\quad q_k'=(\epsilon_r K^2-\mathbf{k}^2)^{\frac{1}{2}}$$
$$q_0=\left(K^2-\mathbf{k}_0^2\right)^{\frac{1}{2}},\quad q_0'=\left(\epsilon_r K^2-\mathbf{k}_0^2\right)^{\frac{1}{2}}. \quad \text{(B6)}$$

The vector $\mathbf{N}=(0,0,1)$ is a unit normal to the horizontal plane and ϵ_r is the surface dielectric permittivity.

The Kirchhoff polarization terms $K_{E,\alpha\alpha_0}$ defined according to Elfouhaily are given by [7]

$$K_{E,11}=D(f_2R_V+f_1R_H),$$
$$K_{E,12}=D(f_3R_V-f_4R_H),$$
$$K_{E,21}=D(f_4R_V-f_3R_H),$$
$$K_{E,22}=D(f_1R_V+f_2R_H). \quad \text{(B7)}$$

where

$$f_1=(\hat{\mathbf{h}}\cdot\hat{\mathbf{K}}_0)(\hat{\mathbf{h}}_0\cdot\hat{\mathbf{K}}),$$
$$f_2=(\hat{\mathbf{v}}\cdot\hat{\mathbf{K}}_0)(\hat{\mathbf{v}}_0\cdot\hat{\mathbf{K}}),$$
$$f_3=(\hat{\mathbf{v}}\cdot\hat{\mathbf{K}}_0)(\hat{\mathbf{h}}_0\cdot\hat{\mathbf{K}}),$$
$$f_3=(\hat{\mathbf{h}}\cdot\hat{\mathbf{K}}_0)(\hat{\mathbf{v}}_0\cdot\hat{\mathbf{K}}),$$
$$D=(K\beta)^2/((\hat{\mathbf{h}}\cdot\hat{\mathbf{K}}_0)^2+(\hat{\mathbf{v}}\cdot\hat{\mathbf{K}}_0)^2) \quad \text{(B8)}$$

in which

$$\hat{\mathbf{K}}_0=(\mathbf{k}_0-q_0\hat{\mathbf{z}})/K,\quad \hat{\mathbf{K}}=(\mathbf{k}+q_k\hat{\mathbf{z}})/K,$$
$$\hat{\mathbf{h}}_0=(\hat{\mathbf{N}}\times\mathbf{k}_0)/\|\mathbf{k}_0\|\quad \hat{\mathbf{h}}=(\hat{\mathbf{N}}\times\mathbf{k})/\|\mathbf{k}\|,$$
$$\hat{\mathbf{v}}_0=\hat{\mathbf{h}}_0\times\mathbf{K}_0,\quad \hat{\mathbf{v}}=\hat{\mathbf{h}}\times\mathbf{K},$$
$$\beta=(1-\hat{\mathbf{K}}\cdot\hat{\mathbf{K}}_0)^{\frac{1}{2}}. \quad \text{(B9)}$$

$\{R_V, R_H\}$ stand for the Fresnel coefficients defined in V and H polarizations, respectively, evaluated at the angle $\arccos(\beta/\sqrt{2})$, and K is the incident wave number.

ACKNOWLEDGMENT

The authors would like to thank anonymous reviewers, whose relevant comments greatly influenced the scope and final appearance of this paper.

REFERENCES

[1] B. F. Kur'yanov, "The scattering of sound at a rough surface with two types of irregularity," *Sov. Phys. Acoust.*, vol. 8, pp. 252–257, 1963.
[2] W. Wright, "A new model for sea clutter," *IEEE Trans. Antennas Propag.*, vol. 16, no. 2, pp. 217–223, Mar. 1968.
[3] A. G. Voronovich and V. U. Zavorotny, "Theoretical model for scattering of radar signals in Ku- and C-bands from a rough sea surface with breaking waves," *Waves Random Media*, vol. 11, pp. 247–269, 2001.
[4] A. G. Voronovich, "Small slope approximation for electromagnetic wave scattering at a rough interface of two dielectric half-spaces," *Waves Random Media*, vol. 4, no. 3, pp. 337–367, 1994.
[5] ——, *Wave Scattering from Rough Surfaces*, 2nd ed, Germany: Springer series on Wave Phenomena, 1999.
[6] ——, "The effect of the modulation Bragg scattering in small-slope approximation," *Waves Random Media*, vol. 12, no. 3, pp. 341–349, 2002.
[7] T. Elfouhaily, S. Guignard, R. Awadallah, and D. R. Thompson, "Local and nonlocal curvature approximation: A new asymptotic theory for wave scattering," *Waves Random Media*, vol. 13, no. 4, pp. 321–337, 2003.
[8] T. Elfouhaily, D. R. Thompson, D. Vandemark, and B. Chapron, "A new bistatic model for electromagnetic scattering from perfectly conducting random surfaces," *Waves Random Media*, vol. 9, no. 1, pp. 281–294, 1999.
[9] J. V. Toporkov and G. S. Brown, "Numerical study of the extended Kirchhoff approach and the lowest order small slope approximation for scattering from ocean-like surfaces: Doppler analysis," *IEEE Trans. Antennas Propag.*, vol. 50, no. 4, pp. 417–425, Apr. 2002.
[10] R. Dashen and D. Wursmer, "Approximate representations of the scattering amplitude," *J. Math. Phys.*, vol. 32, no. 4, pp. 986–966, 1991.
[11] T. Elfouhaily, M. Joelson, S. Guignard, and D. R. Thompson, "Analytical comparison between the surface current integral equation and the second-order small-slope approximation," *Waves Random Media*, vol. 13, no. 3, pp. 165–176, 2003.
[12] T. Elfouhaily, S. Guignard, and D. R. Thompson, "Formal tilt invariance of the local curvature approximation," *Waves Random Media*, vol. 13, no. 4, p. L711, 2003.
[13] M. I. Charnotskii and V. I. Tatarskii, "Tilt-invariant theory of scattering by rough surface," *Waves Random Media*, vol. 5, no. 4, p. 36180, 1995.
[14] T. Elfouhaily and C. A. Guérin, "Critical survey of approximate scattering wave theories from random rough surfaces," *Waves Random Media*, vol. 14, no. 4, pp. R1–R40, 2004. Topical review.
[15] T. Elfouhaily, B. Chapron, K. Katsaros, and D. Vandemark, "A unified directional spectrum for long and short wind-driven waves," *J. Geo. Res.*, vol. 102, no. C7, pp. 781–796, 1997.
[16] V. Voronovich, U. Zavorotny, and V. G. Irisov, "Sea-roughness spectrum retrieval from radar and radiometric measurements," in *Int. Geos. Remote Sens. Symp.*. Piscataway, NJ, 2000, pp. 3102–3104.
[17] C. Bourlier and G. Berginc, "Microwave analytical backscattering models from randomly rough anisotropic sea surface—Comparison with experimental data in C and Ku bands," in *Progress in Electromagnetic Research*, Y. Zhang and T. M. Grzegorczyk, Eds. Cambridge, MA: EMW, 2002, vol. 37, pp. 31–78.
[18] S. T. McDaniel, "Small-slope predictions of microwave backscatter from the sea surface," *Waves Random Media*, vol. 11, pp. 343–360, 2001.
[19] G. Soriano, C. A. Gurin, and M. Saillard, "Scattering by two-dimensional rough surface: Method comparison," *Waves Random Media*, vol. 12, no. 1, pp. 63–83, 2002.
[20] S. L. Broschat and E. I. Thorsos, "An investigation of the small slope approximation for scattering from rough surfaces. Part II: Numerical studies," *J. Acoust. Soc. Amer.*, vol. 101, no. 5, pp. 2615–2625, 1997.
[21] J. T. Johnson, "A numerical study of low-grazing-angle backscatter from ocean-like impedance surfaces with the canonical grid method," *IEEE Trans. Antennas Propag.*, vol. 46, no. 1, pp. 114–120, Jan. 1998.
[22] H. Kim and J. T. Johnson, "Radar image studies of an ocean-like surface," *Microwave Opt. Tech. Lett.*, vol. 30, no. 6, pp. 381–384, 2001.
[23] G. Berginc, "Small-slope approximation method: A further study of vector wave scattering from two-dimensional surfaces and comparison with experimental data," in *Progress in Electromagnetic Research*, Y. Zhang and T. M. Grzegorczyk, Eds. Cambridge, MA: EMW, 2002, vol. 37, pp. 251–287.
[24] M. S. Gilbert and J. T. Johnson, "A study of the higher-order small-slope approximation for scattering from a Gaussian rough surface," *Waves Random Media*, vol. 13, no. 2, pp. 137–149, 2003.
[25] W. Ellison, A. Balana, G. Delbos, K. Lamkaouchi, L. Eymard, C. Guillou, and C. Prigent, "New permittivity measurements of seawater," *Radio Sci.*, vol. 33, pp. 639–648, 1998.

[26] A. K. Fung, C. Zuffada, and C. Y. Hsieh, "Incoherent bistatic scattering from the sea surface at L-band," *IEEE Trans. Geos. Remote Sens.*, vol. 39, no. 5, pp. 1006–1012, 2001.
[27] E. Thorsos, "Acoustic scattering from 'PiersonMoskowitz' sea surface," *J. Acoust. Soc. Amer.*, vol. 88, pp. 335–349, 1990.
[28] C. L. Rino, T. L. Crystal, A. K. Koide, H. D. Ngo, and H. Guthart, "Numerical simulation of backscatter from linear and nonlinear ocean surface realizations," *Radio Sci.*, vol. 26, pp. 51–71, 1991.
[29] D. J. Donohue, H.-C. Ku, and D. R. Thompson, "Application of iterative moment-method solutions to ocean surface radar scattering," *IEEE Trans. Antennas Propag.*, vol. 46, no. 1, pp. 121–132, Jan. 1998.
[30] C. Bourlier and G. Berginc, "Shadowing function with single reflection from anisotropic Gaussian rough surface. Application to Gaussian, Lorentzian and sea correlations," *Waves in Random Media*, vol. 13, no. 1, pp. 27–58, 2003.
[31] W. H. Press, S. A. Teukolsky, W. T. Vetterling, and B. P. Flannery, *Numerical Recipies in C*, 2nd ed. Cambridge, MA: Cambridge Univ. Press, 1992, ch. 2, p. 77.

Christophe Bourlier (M'99) was born in La Flèche, France, on July 6, 1971. He received the M.S. degree in electronics from the University of Rennes, France, in 1995 and the Ph.D. degree from the Système Electronique et Informatique (SEI) Laboratory, Institut de Recherche et d'Enseignement Supèrieur aux Techniques de l'Electronique (IRESTE), University of Nantes, France, in 1999.

While at the University of Rennes, he was with the Laboratory of Radiocommunication where he worked on antennas coupling in the VHF-HF band. Now, he is with the Radar Team at the Institut de Recherche en Electrotechnique et Electronique de Nantes Atlantique, (IREENA), at Ecole polytechnique de l'université de Nantes, France, where he works as a Researcher of the Centre National de la Recherche Scientifique (CNRS) on the problem of the electromagnetic wave scattering from rough surfaces in microwave and infrared bands. He is the author of more than 40 journal articles and conference papers.

Nicolas Déchamps was born in Provins, France, in 1977. He received the Engineering Degree from Ecole Centrale de Nantes, Nantes, France, the M.S. degree in automation and applied computer science from the Communications and Cybernetic Research Institute of Nantes (IRCCyN), and the Ph.D. degree in physics from the Institut de Recherche en Electrotechnique et Electronique de Nantes Atlantique, (IREENA), in 2004, where he worked on fast numerical methods for numerical simulations of scattering from multilayers separated by one-dimensional (1-D) rough interfaces. He is currently working toward a Postdoctoral degree in chemical engineering and applied chemistry at the University of Toronto, Toronto, ON, Canada.

He has worked on fast numerical methods for numerical simulations of scattering from multilayers separated by 1-D rough interfaces.

Gérard Berginc was born in Etain, France, on March 25, 1959. He received the Dipl.Ing. degree from the Ecole Nationale Supérieure de Physique, Marseille, France, and the DEA of Theoretical Physics (with honors) from the University of Aix-Marseille, France, in 1983.

He joined Thomson-CSF, France. From 1985 to 1987, he was a Research Engineer and was involved in the development of radar performance calculation methods. From 1987 to 1990, he worked at Mothesim, France, as Head of the Underwater Acoustic Research Department and as Consultant for modeling electromagnetic phenomena in radar and space systems. From 1990 to 1991, he was with Thomson-CSF DAS as a technical expert in electromagnetic calculation methods. In 1991, he joined Thalès Optronique, Guyancourt, France, where he is currently the Leader of a research group in the Research and Development Department. He is author of more than 60 journal articles, conference papers, book chapters, and holder of 20 patents. His research activities include diffraction theory, high frequency asymptotics, rough surface and random media scattering, localization effects, and frequency selective surfaces.

Dr. Berginc is a Member of the Electromagnetics Academy and the SPIE. He is a correspondent of the International Scientific Radio Union (URSI) Commissions B and F.